Contact Mechanisms of Transfer Layered Surface During Sliding Wear of Amorphous Carbon Film

X. Fan

D. F. Diao[1]
e-mail: dfdiao@mail.xjtu.edu.cn

Key Laboratory of Education Ministry for Modern Design and Rotor-Bearing System, School of Mechanical Engineering, Xi'an Jiaotong University, Xi'an 710049, China

The contact mechanisms of a transfer layered surface during sliding wear of a Si_3N_4 ball against the amorphous carbon film were investigated. In this study, amorphous carbon films were deposited by electron cyclotron resonance plasma sputtering technique. The dependence of friction coefficient and wear life of the films on transfer layer was tested with pin-on-disk tribometer. Wear tracks and the transfer layered surfaces at different friction coefficient stages were observed with scanning electron microscope and measured with energy dispersive spectrometer In order to clarify the contact mechanisms of a transfer layered surface, three contact models of initial high friction coefficient stage without transfer layer (state I), transfer layer forming stage with friction coefficient decreasing (state II), and transfer layered surface stable sliding stage with low friction coefficient (state III) were proposed, and the contact stresses (normal stress, shear stress, von Mises stress) of the three contact states were calculated by using finite element analysis. The results demonstrated that a transfer layer formed at the contact interface and gradually decreased the maximum contact stresses, which contributed to the long wear life of amorphous carbon films. [DOI: 10.1115/1.4004999]

Keywords: contact mechanism, transfer layer, amorphous carbon film, friction and wear finite element analysis

1 Introduction

Amorphous carbon films exhibit a low friction coefficient and long wear life for tribological applications to provide protection for counterparts [1]. Many studies on the friction and wear mechanisms of amorphous carbon films have been published. Friction and wear behaviors were affected by the intrinsically chemical, structural, and mechanical properties of the films, as well as the externally chemical, physical and mechanical interactions between the amorphous carbon film surfaces and their surroundings [2–4]. The dangling bond mechanism has been studied by Eryilmaz et al. [5] in which it was found that passivation of dangling bonds of surface carbon atoms by oxygen reduced the extent of adhesive interactions, and therefore contributed to the reduced friction and wear. Heimberg et al. [6] studied the time and speed effects on the super low friction behavior (0.003–0.008) of amorphous carbon films, and the results indicated that gas-surface interactions played an important role in inhibiting super low friction. The forming or consuming of a transfer layer on the sliding surfaces and the physical and chemical natures of such films also influence friction. Sugimoto and Miyake [7] suggested that a low friction coefficient below 0.01 was achieved by the formation of oriented hydrocarbons on the ball surface with transferred hydrocarbon molecules. Fukui et al. [8] used TOF-SIMS to explore the chemical nature of a transfer layer generated during tribological tests of hydrogenated amorphous carbon films. They reported that the transfer layer was primarily made of hydrocarbon macromolecules which suggested the formation of a polymer-like self-lubricating layer on sliding surfaces. When amorphous carbon films slide with a counter ball, the contact mechanism is smoothing, followed by building up a transfer layer. The transfer layer mostly formed on the surfaces of uncoated counter balls, sliding against the amorphous carbon films [9]. Studies have noted that co-sliding motion took place between the transfer layer on the ball and the film, and the velocity accommodation mode, interfacial sliding, and low interfacial shear strength resulted in low friction [10]. The discussions above on contact mechanisms during sliding wear of transfer layered surfaces mainly focused on the physical and chemical properties of transfer layer.

From the viewpoint of engineering application of amorphous carbon films, it is well known that the maximum contact stresses (maximum normal stress, maximum shear stress and maximum von Mises stress) are important factors for the design of amorphous carbon films in tribological applications because surface damage, delamination, and spalling of the films are usually caused by these maximum stresses. O'Sullivan et al. [11] calculated the contact stresses when an elastic spherical indenter sliding against a three-dimensional elastic half-space with a single layer. Diao et al. [12,13] used the finite element analysis method to present a simple equation that related maximum tensile stress at the film surface to friction coefficient, relative layer thickness, and elastic modulus ratio of layer to substrate. Furthermore, the effects of friction coefficient on the maximum tensile and shear stresses at the layer interface have also been studied. In recent years, the studies of contact mechanisms of film surfaces mainly include three-dimensional finite element analysis of elastic and plastic layered half-space [14–16], the influence of surface roughness on the magnitude and depth of maximum shear stress in the layer [17], the effect of residual stress in the surface layer on the deformation of elastic-plastic layered half-space due to indentation and sliding contact [18], and also the thermal-mechanical finite element analysis on the stress and temperature distributions in the layered half-space during sliding contact [19,20]. However, the contact stress distributions of amorphous carbon films with a transfer layer changing at the contact interface during sliding wear have not been studied.

The purpose of this paper is to study the contact mechanisms of transfer layered surface during sliding wear of amorphous carbon film. For this purpose, carbon films are deposited with Electron Cyclotron Resonance (ECR) plasma sputtering technique on silicon substrate, and the nano structures are observed and analyzed by High Resolution Transmission Electron Microscope (HRTEM),

[1]Corresponding author.

Contributed by the Tribology Division of ASME for publication in The Journal of Tribology. Manuscript received December 27, 2010; final manuscript received August 31, 2011; published online October 19, 2011. Assoc. Editor: Mitjan Kalin.

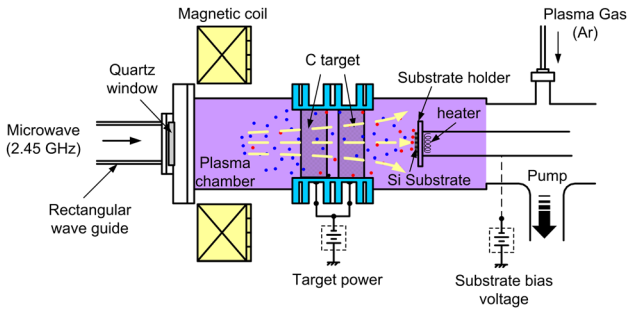

Fig. 1 Schematic illustration of ECR Plasma Sputtering Equipment

X-ray Spectroscopy (XPS) and UV Raman spectrometer. Friction coefficients and wear lives of the films are obtained from a Pin-on-Disk (POD) tribometer, the wear tracks on film surface and the transfer layers on a Si_3N_4 ball surface are observed and measured with Scanning Electron Microscopy (SEM), Energy Dispersive Spectrometer (EDS), and a nano indenter. According to the experimental results, contact models of different friction coefficient stages are proposed to analyze the contact stresses of transfer layered amorphous carbon film during sliding wear by using Finite Element Analysis (FEA).

2 Experimental Details

2.1 Preparation of Amorphous Carbon Films. Carbon films were deposited on p-type ⟨100⟩ oriented silicon substrate with ECR plasma sputtering technique. Figure 1 shows the schematic illustration of ECR plasma sputtering equipment. A silicon wafer with the size of 20 mm × 20 mm × 0.52 mm was degreased in acetone and cleaned with absolute ethyl alcohol, then fixed onto the substrate holder and put into the vacuum chamber. When the chamber was pumped down to the background pressure of 3×10^{-4} Pa, argon was inflated, keeping the working pressure to be 0.04 Pa. The heater under substrate holder was heated to 400 degrees C within 10 mins and the substrate temperature was kept at 400 degrees C during deposition and after the deposition for one hour. Argon plasma was generated when the 2.45 GHz microwave and divergent magnetic field were activated, and electron cyclotron resonance was formed at the place where magnetic flux density was 875 G. Then, plasma sputtered the carbon target with a discharge voltage of −300 V. Finally the sputtered carbon atoms were deposited on the silicon substrate with substrate bias voltage (V_b) ranging from −10 V to +50 V for 25 mins. The thickness and nano structure of the prepared carbon films were evaluated with HRTEM, XPS and Raman, and results are shown in Fig. 2.

Figure 2(*a*) shows the cross-sectional TEM picture of ECR carbon film with substrate bias voltage of +10 V; the thickness was 113 nm. The diffraction pattern on the top right corner shows that the nano structure was amorphous, and the film was isotropic. From the cross-sectional TEM picture, it is clear that the top surface structure is the same with the bulk film, and the ECR carbon films were structurally uniform. Raman spectrum of the ECR carbon film in Fig. 2(*b*) consisted of a *G* peak at 1590 cm^{-1}, and a *D* peak at about 1350 cm^{-1}. According to the Chhowalla et al. [21], the appearance of the *D* peak indicated that the sp^2 bonds began to form aromatic clusters well before a significant decrease in the sp^3 fraction occurred for the amorphous carbon films deposited with high temperature, Raman result implied that ECR carbon films had small disordered crystallites in the amorphous structure. The sp^2 and sp^3 carbon hybridizations of amorphous carbon films were quantitatively obtained by using the curve fitting method through decomposing the XPS C1s spectrum into Gaussian-Lorentzian distributions, as shown in Fig. 2(*c*). During peak fitting, except for the sp^2 and sp^3 carbon hybridizations at binding energy of 284.4 and 285.2 eV respectively, another two peaks of much smaller

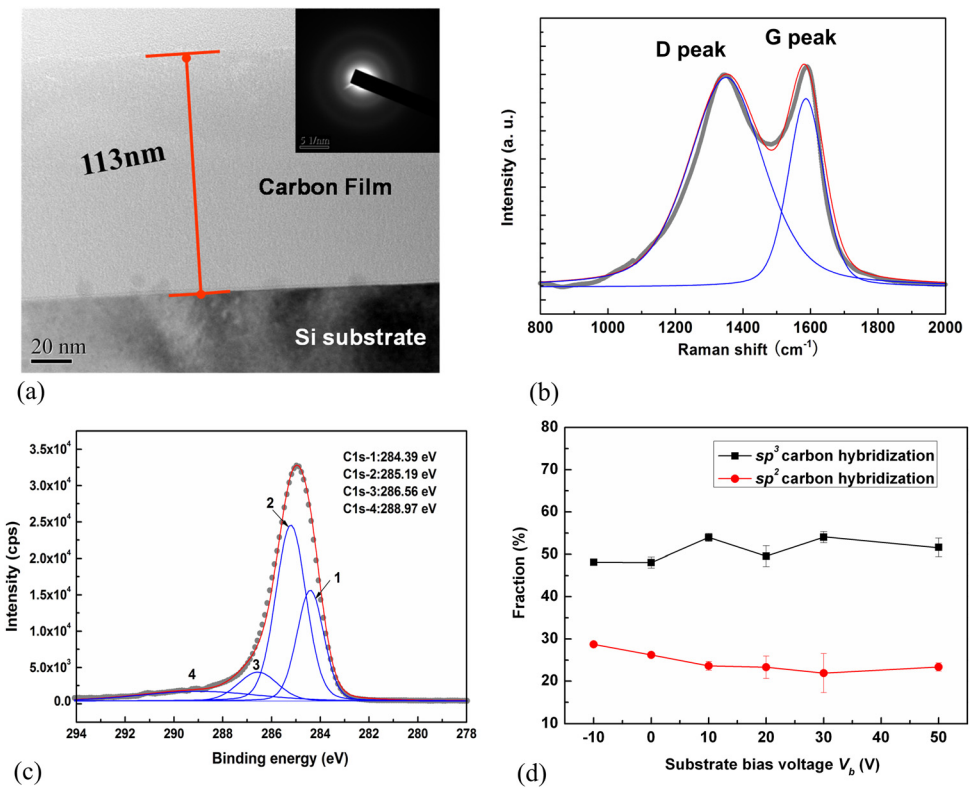

Fig. 2 Characterizations of the ECR carbon film. (*a*) Cross-sectional HRTEM picture; (*b*) Peak fitting result of Raman spectrum (V_b = + 10 V); (*c*) Peak fitting result of C 1 s spectrum (V_b = + 10 V); (*d*) The fractions of sp^3 and sp^2 bonds by XPS.

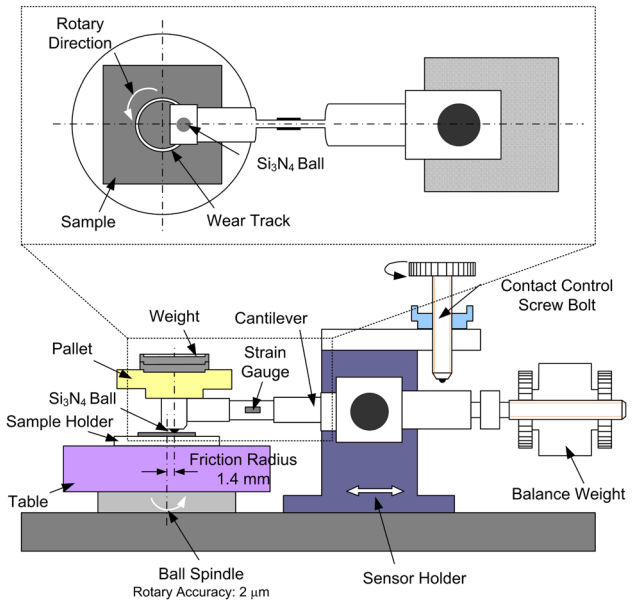

Fig. 3 Schematic illustration of Pin-on-Disk tribometer

intensity at 286.6 and 288.8 eV have also been noticed which were attributed to some carbon atoms bonded to N, O, and other adsorbents from air on the film surface. The results of sp^2 and sp^3 carbon hybridizations are shown in Fig. 2(*d*). The fractions of sp^3 bonds were around 50% which were in the typical range of various amorphous carbon films (20%–80%).

2.2 Pin-on-Disk Tribotest. The friction coefficients and wear lives of amorphous carbon films were tested with a Pin-on-Disk tribometer, as shown in Fig. 3, which was operated in room temperature environment of 21 degrees C and humidity of 45%. The rigid Si_3N_4 ball with radius (R) of 3.17 mm was chosen as the counter ball, which was widely used in industrial applications as a ball bearing with low friction [22,23]. The disk of amorphous carbon film was fixed on the sample table. Before the test, the ball and disk were cleaned with absolute ethyl alcohol, and balance weight was adjusted to keep the cantilever horizontality. A normal load (W) of 2 N was applied through putting weight on the pallet, and the weight was imposed by slowly adjusting the Screw Bolt in order to insure that there was no impact on the film surface. During the test, the disk was rotated at a speed of 180 rpm controlled by a ball spindle with the rotary accuracy of 2 μm, which can keep the linear speed of all contact points (V) to be 26 mm/s in this paper. The distance between the axis of Si_3N_4 ball and the axis of rotary spindle determined the radius of friction circle, which was 1.4 mm in our tests. Strain gauge stuck on the cantilever was used to measure the friction force with the accuracy of 0.02 N. After tests at chosen friction cycles, SEM and EDS were used to observe and measure the wear tracks on the film surface and the transfer layers on the Si_3N_4 ball surface. The elastic moduli of the carbon film, transfer layer and Si_3N_4 ball were measured with a TriboScope nano-mechanical tester.

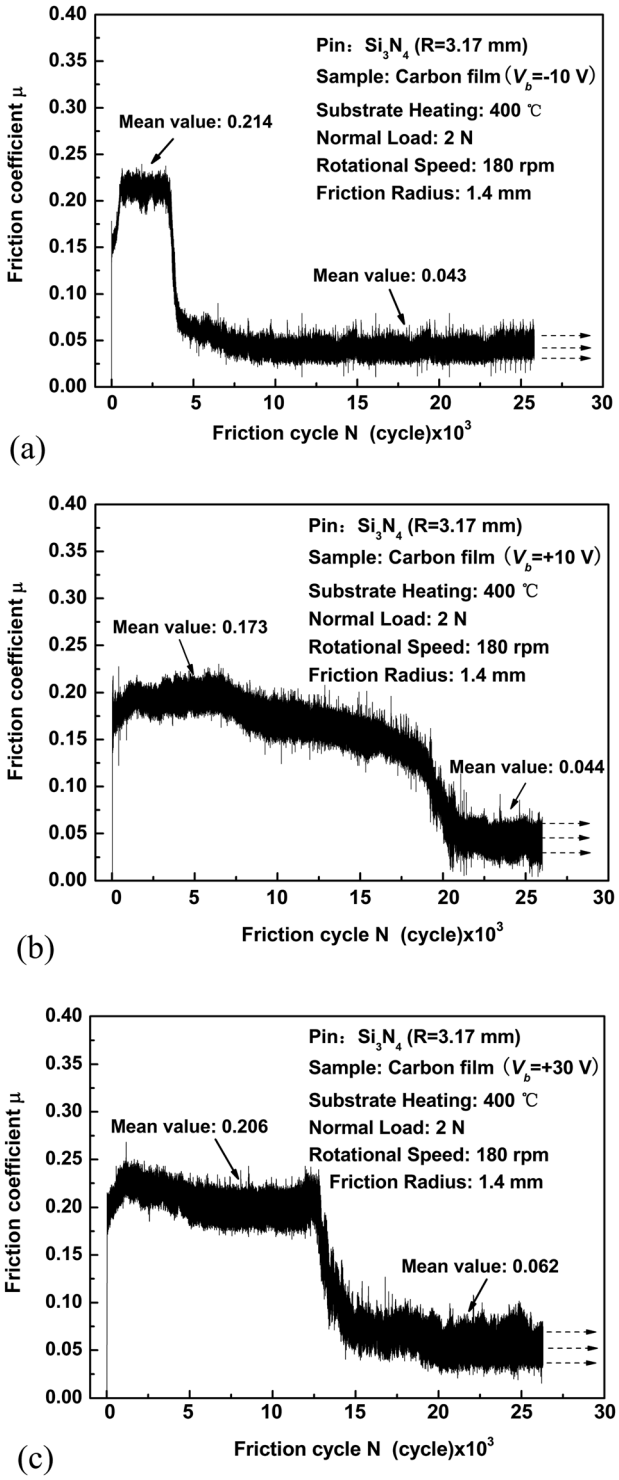

Fig. 4 Typical friction curves of the amorphous carbon films with substrate bias voltages of −10 V (*a*), + 10 V (*b*), and + 30 V (*c*)

3 Experimental Results

3.1 Tribological Properties of Amorphous Carbon Films. Three typical friction curves of amorphous carbon films deposited with substrate bias voltages of −10 V, + 10 V, and + 30 V are shown in Fig. 4. The friction coefficient first kept at relative high stage with mean values of 0.214, 0.173 and 0.206 in Figs. 4(*a*), 4(*b*) and 4(*c*) respectively, then, it dropped down to low stage after certain friction cycles with mean values of 0.043, 0.044, and 0.062 respectively, and the films were not worn out at the end of the test with 26 000 cycles.

The mean friction coefficients and wear lives of amorphous carbon films with different substrate bias voltages are summarized in Fig. 5. The mean high friction coefficients were near the value of 0.2, and the mean values of low friction coefficients were around 0.05. During the tests, when the friction cycle of amorphous carbon films exceeded 26 000 cycles, the sliding processes were stopped (see the up arrows in Fig. 5). The contact mechanisms for

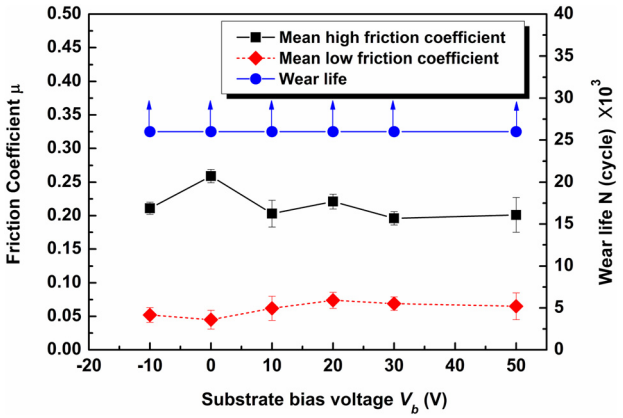

Fig. 5 Friction coefficients and wear lives of the amorphous carbon films with different substrate bias voltages

long wear lives of amorphous carbon films will be studied with the characteristics of friction coefficient curves in the following section.

3.2 Transfer Layered Surfaces. A typical amorphous carbon film with bias voltage of +10 V was chosen for further analysis. In order to study the contact mechanisms during sliding wear, the wear tracks at different friction coefficient stages are shown in Fig. 6. At the high friction coefficient stage, only a slight sliding track can be seen on the film surface, and the width was 74 μm (Fig. 6(*a*)). At the friction coefficient decreasing stage, the wear track with width of 96 μm was clearer, and small flaking of the film appeared at the sides of the wear track (Fig. 6(*b*)). When the friction coefficient stabilized at low value, the width of the wear track was 108 μm; a large area of flaking films can be seen at the side of the wear track, and there were small wear debris in the wear track (Fig. 6(*c*)).

The forming and changing process of the transfer layer on the Si_3N_4 ball surface during sliding wear was characterized with EDS. Figure 7 shows the test positions on the surfaces of the amorphous carbon film side (see Fig. 7(*a*)) and the transfer layered Si_3N_4 ball side (see Fig. 7(*b*)). Test results of Site 1 to 5 are shown in Fig. 8. At the high friction coefficient stage, carbon content of the sliding track was nearly the same with that of as-deposited film, and only a slight sliding track can be seen from the film surface (Fig. 6(*a*)), correspondingly, on the surface of the Si_3N_4 ball, only 0.01% carbon was tested which was supposed to be the absorbed carbon atoms. No transfer layer formed at this stage. Although there was no wear of film at this stage, the carbon content of the film side was only about 41%; this is because the film thickness was only about a hundred nanometers, while the EDS penetrate depth was deeper than the film thickness and reached the silicon substrate. In our test, the other left percentages were substrate material of silicon with a bit of oxygen. At the friction coefficient decreasing stage, the carbon content at Site 2 decreased (see Fig. 8(*a*)), and the accumulated carbon on the center of the Si_3N_4 ball surface was up to 9.22%. The carbon atoms on the Si_3N_4 ball surface was considered to be the transfer layer and came from the carbon film because both the silicon substrate and the Si_3N_4 ball did not contain carbon atoms at all. Therefore, a transfer layer formed on the Si_3N_4 ball surface at this stage. The transfer layer thickness was estimated according to the carbon film thickness observed by TEM and the carbon content of as-deposited film measured by EDS, which was approximately 0.025 μm in this stage. At the low friction coefficient stage, the carbon content in the wear track did not change comparing with the friction coefficient decreasing stage, while the content at the transfer layered Si_3N_4 surface decreased to 7.44%. This means that the transfer layer thickness in the contact center decreased and was approximately 0.02 μm at this stage. The estimated transfer layer thickness of about

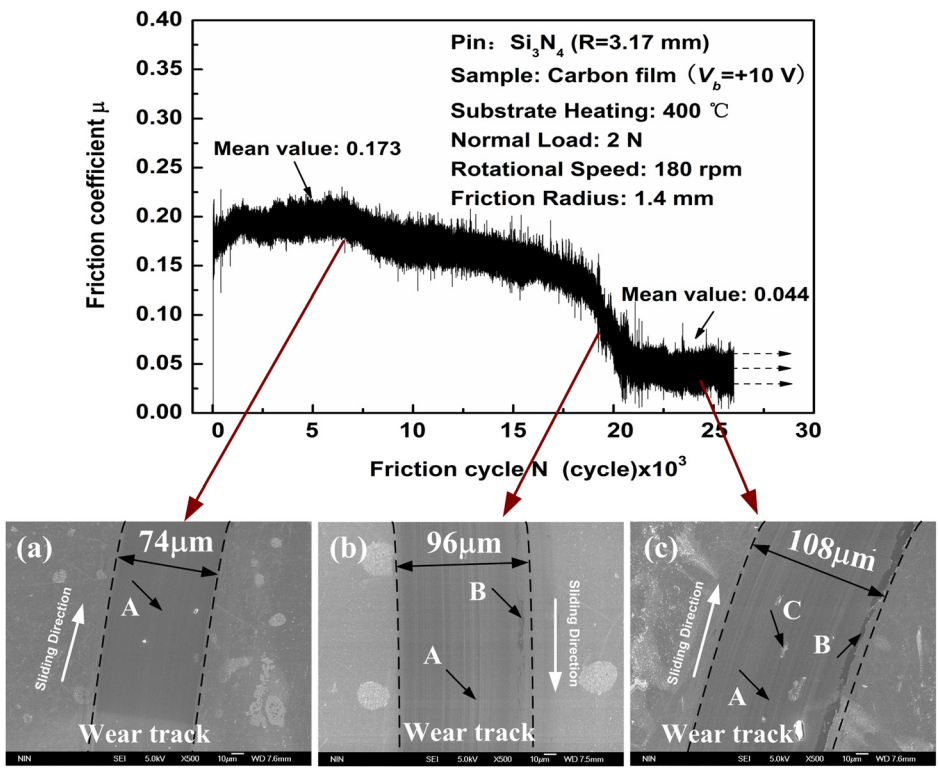

Fig. 6 Wear tracks on the amorphous carbon film surfaces at three different stages. 6(*a*) High friction coefficient stage; (*b*) friction coefficient decreasing stage; (*c*) low friction coefficient stage (A: grooves, B: flaking, C: wear debris).

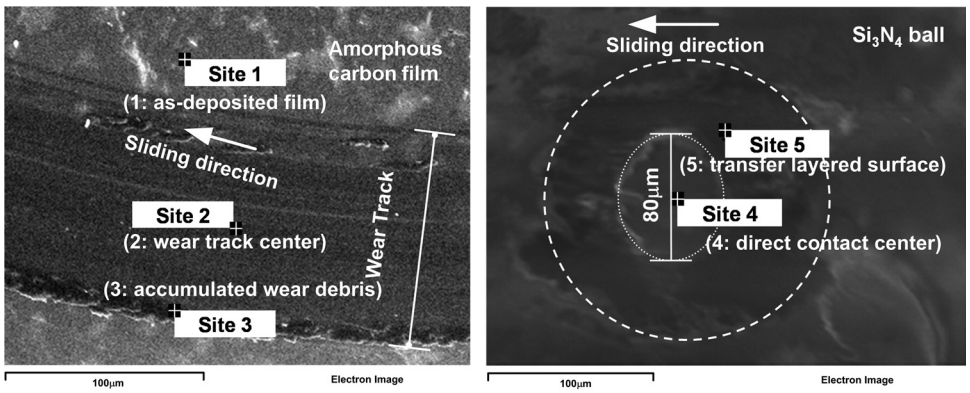

Fig. 7 EDS testing positions on the surfaces of the amorphous carbon film (*a*) and the Si_3N_4 ball (*b*)

20 nm was nearly the same with the AFM measurement results by Tokoroyama et al. [24].

In order to get the elastic moduli of the carbon films and transfer layer, a nano indenter with a Berkovich tip was used to obtain the load-displacement curve under the maximum load of 500 μN. The curves with loading and unloading processes on amorphous carbon film, transfer layer and the Si_3N_4 ball are shown in Fig. 9. When the same maximum indentation load was reached, full elastic recovery was found for the Si_3N_4 ball, large elastic recovery can be observed for carbon film, and a plastic indentation depth of 18 nm appeared for the transfer layer, which was much larger than that of the carbon film and the Si_3N_4 ball. Based on the load-displacement curves, the elastic moduli were obtained with the analysis method given by Oliver and Pharr [25]. The values were 142.3 GPa, 100.1 GPa and 336.9 GPa for amorphous carbon film, the transfer layer and the Si_3N_4 ball respectively.

Based on the test results of the transfer layered surface and wear track, contact states at the initial high friction coefficient stage without transfer layer (state I), transfer layer forming stage with friction coefficient decreasing (state II), and transfer layered surface stable sliding stage with low friction coefficient (state III), were proposed as shown in Figs. 10(*a*), 10(*b*), and 10(*c*) respectively. The film worn out stage (state IV) also existed (Fig. 10(*d*)), however, since the film has been worn out at this state, the contact mechanism was not included in this study. At state I, the Si_3N_4 ball directly contacted with the film surface without a transfer layer; according to the sliding track width in Fig. 6(*a*), the contact width ($2a$) was 74 μm. At state II, a transfer layer was formed at the interface between the film and the Si_3N_4 ball; the transfer layer length was 96 μm ($2b_1$) according to the wear track width in Fig. 6(*b*), and the thickness at the contact center was 0.025 μm (h_1) as mentioned above. The transfer layer got thinner and wider at state III, which was 108 μm ($2b_2$) long and 0.02 μm thick (h_2), and then the film was worn out (state IV). During the sliding wear process, the contact surfaces generated wear, which changed the contact geometry, wear contact width between the ball and film increased with the increasing number of friction cycles, which was larger than the initial contact width [26]. In the present study, due to the long sliding distance, the wear of the Si_3N_4 ball generated and the surface profile of ball changed (as shown in the schematic diagram in Figs. 8(*b*) and 8(*c*)). It should be noticed that according to our observation, as shown in Fig. 7(*b*), the wear contact width increased to 80 μm ($2b_0$) at states II and III. The four contact states decide the variation of friction coefficient and wear life of the films. Therefore, it is necessary to study the contact stresses of the transfer layered amorphous carbon films during sliding wear based on the three contact states before the film is worn out.

4 Finite Element Analysis

To better understand the contact mechanisms of transfer layered surface, the contact stress distributions (normal stress σ_{xx}, shear stress σ_{xy}, and von Mises stress σ_{von}) along the surfaces of

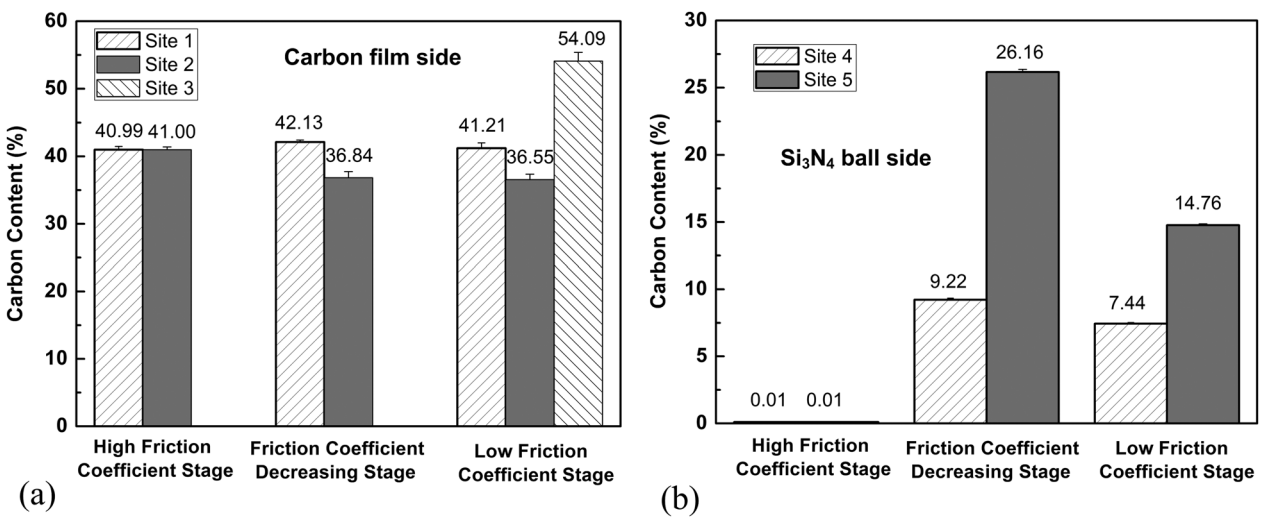

Fig. 8 Carbon contents of the amorphous carbon film (*a*) and the Si_3N_4 ball (*b*) tested by EDS

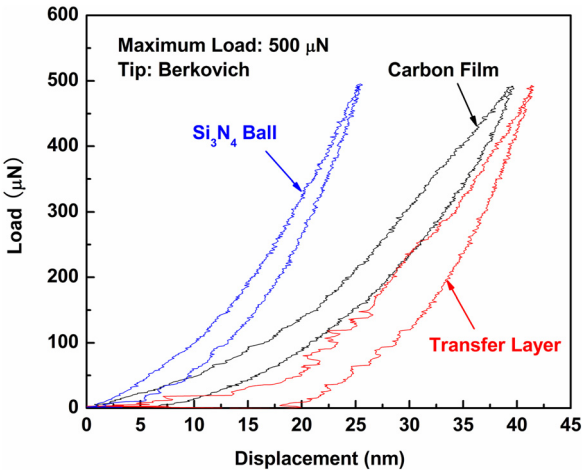

Fig. 9 Load-displacement curves of the amorphous carbon film, transfer layer and the Si_3N_4 ball

amorphous carbon film at three contact states (state I, state II and state III as proposed above) are calculated by finite element analysis.

4.1 Finite Element Analysis Modeling. Figures 11(*a*) and 11(*b*) show the schematic FEA models for states I, II and III. In order to show the contact area and transfer layer clearly, part of the finite element meshes in large scale is shown in Fig. 11(*c*). The lower part of the finite element model was 1000 μm long (BC) by 500.113 μm thick (AB, CD) to represent a semi-infinite body with 0.113 μm thick film and 500 μm thick silicon substrate. For the boundary conditions, the displacements of elements on borderline AB and CD were fixed in the x direction, and those on borderline BC were fixed in the y direction.

In order to simulate the transfer layered surface of amorphous carbon films, the key factors including friction coefficient, contact width, transfer layer size (length and thickness), and contact pressure are needed, which will change during sliding wear. The actual friction coefficients, contact widths, and transfer layer sizes at three contact states were given by the experimental results, as shown in Table 1.

At state I, the film was very thin comparing with the silicon substrate, and the elastic modulus of carbon film (142.3 GPa) was close to that of silicon substrate (131 GPa), thereby, elliptical contact pressure distribution can be used as follows:

$$P(x) = \begin{cases} P_{\max}\sqrt{1-(x/a)^2} & (|x| \le a) \\ 0 & (|x| > a) \end{cases} \quad (1)$$

where $P_{\max}$ is the maximum contact pressure; a is the half contact width.

At states II and III, considering that the wear contact width changed on the Si_3N_4 ball surface and the transfer layer formed, pressure distribution changed. According to the FEM analysis by Ding [26] and the numerical calculation by Nowell [27], when the

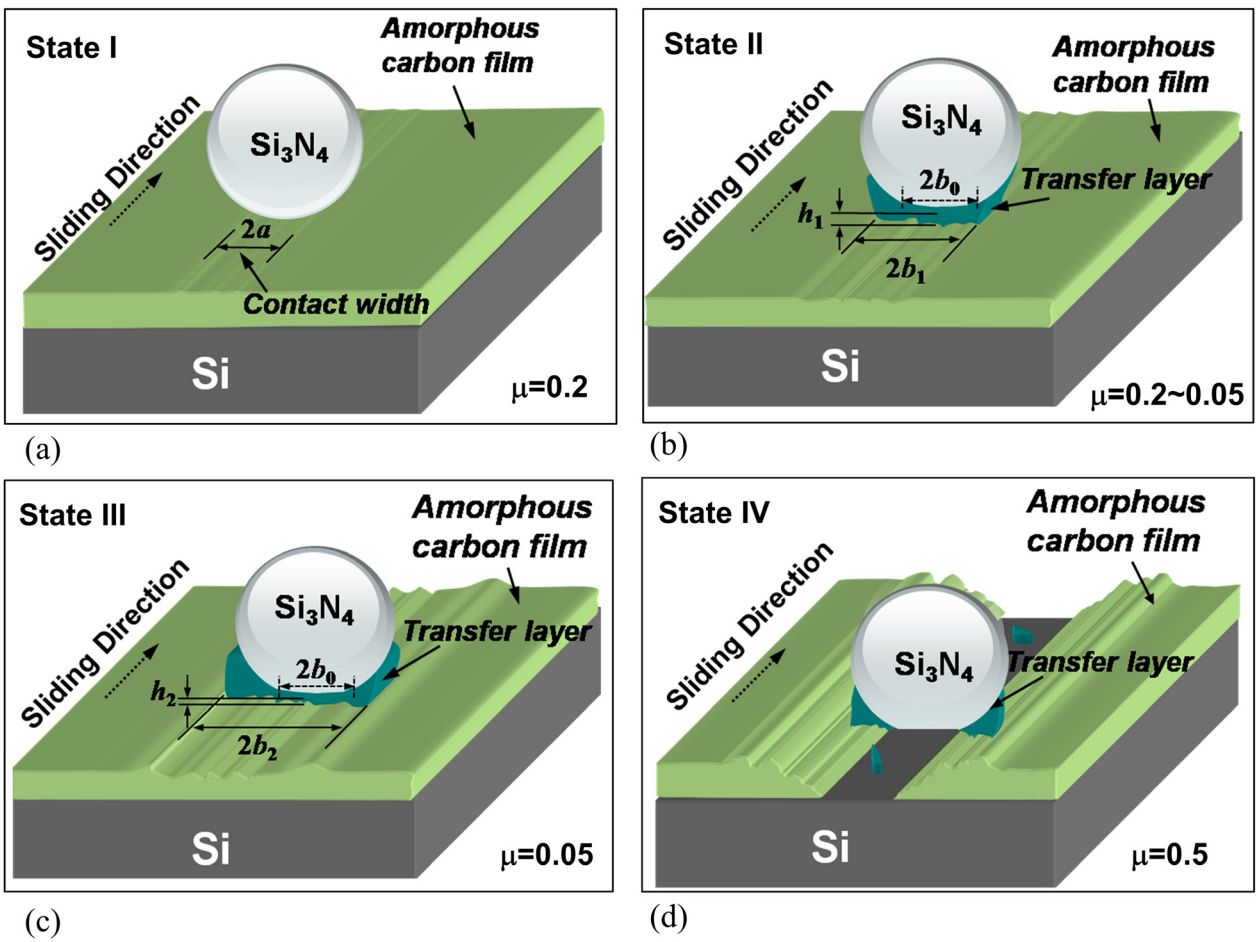

Fig. 10 Schematic contact states during the sliding wear process. (*a*) Initial high friction coefficient stage; (*b*) Friction coefficient decreasing stage; (*c*) Low friction coefficient stage; (*d*) Amorphous carbon film worn out stage.

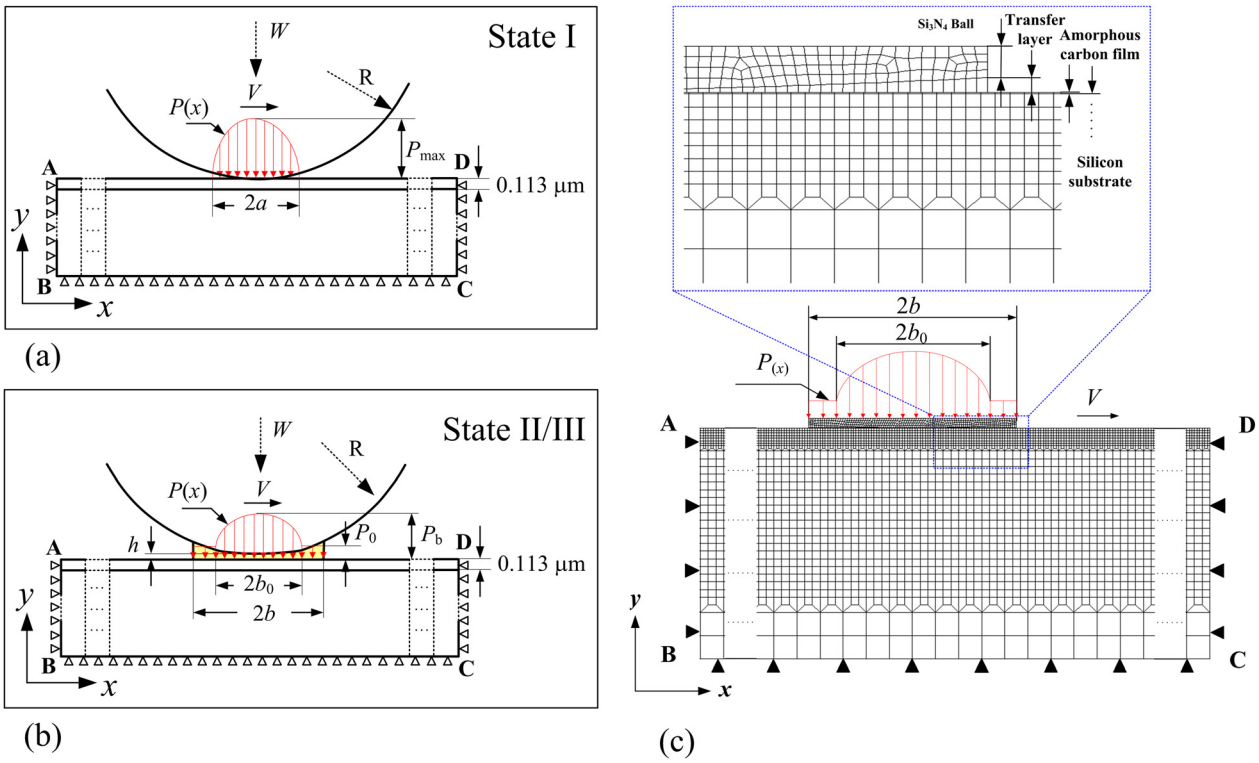

Fig. 11 FEA schematic models of state I without a transfer layer (*a*), state II/III with different sizes of transfer layers (*b*) and mesh models (*c*)

contact width grew during wear, the peak pressure fell before turning into the uniform distribution. The variation of the peak pressure with contact width as wear proceeds is given as [27]:

$$\frac{P_{\max}}{P_b} = \frac{\pi}{4} \times \frac{a}{b_0} \tag{2}$$

where, $P_{\max}$ is the maximum contact pressure, P_b is the peak contact pressure when contact width grows during wear, and b_0 is the half wear contact width. The wear contact width ($2b_0$) was obtained to be 80 μm at states II and III, and then $P_b = 0.726P_{\max}$.

It is clear how the pressure is distributed when the ball is directly in contact with the film surface. However, when a transfer layer forms at the contact interface, the surrounding transfer layer also shares the pressure. As the transfer layer thickness in the wear track ($|x| < b_0$) was much thinner when compared with the diameter of the Si_3N_4 ball, the pressure was also elliptically distributed in this part. On the other hand, with the effect of the surrounding transfer layer, the pressure consecutively transformed to a uniform distribution in the range of $b_0 \le |x| \le b$, because the transfer layer was generated by the accumulation of wear debris, and it was thicker and softer in this area. The contact pressure distribution of states II and III is expressed as follows:

Table 1 Friction coefficients, contact widths, and transfer layer sizes of the three contact states

State	Friction coefficient (μ)	Half contact width, μm	Transfer layer length ($2b$), μm	Transfer layer thickness (h), μm
State I	0.2	(a) 37	–	–
State II	0.2 ~ 0.05	(b_0) 40	96	0.025
State III	0.05	(b_0) 40	108	0.02

$$P_{(x)} = \begin{cases} (P_b - P_0)\sqrt{1 - (x/b_0)^2} + P_0 & (|x| \le b_0) \\ P_0 & (b_0 \le |x| \le b) \end{cases} \tag{3}$$

As mentioned, P_b is the peak contact pressure when contact width grows during wear; P_0 is uniform pressure, and b_0 is the half wear contact width. P_0 was obtained based on the fact that the integral of pressure distribution $P_{(x)}$ at different contact states was equal to the normal force W which acted on the Si_3N_4 ball during sliding wear process. This can be calculated as:

$$P_0 = \frac{\pi a - 0.726\pi b_0}{4b - \pi b_0} \times P_{\max} \tag{4}$$

where, $a = 37\,\mu$m, $b_0 = 40\,\mu$m, $b_1 = 48\,\mu$m for state II and $b_2 = 54\,\mu$m for state III, then, P_0 was calculated to be $0.377P_{\max}$ for state II and $0.277P_{\max}$ for state III. The pressure distributions of three contact states are shown in Fig. 12.

A commercial code (ANSYS 10.1) was used to calculate the contact stresses at the transfer layered amorphous carbon film surface. Default contact stiffness of contact interface was applied in the finite element model. The automatic increment option in each step was used. The mesh was composed of a 2-D four-nodded coupled area element (PLANE 13), and a two-node surface contact element. CONTACT 171 was used to represent contact and sliding between the target surface and a deformable surface. Contact occurred when the element surface penetrated one of the target segment elements on a specified target surface. The target surface was defined by TARGET 169 for the associated contact elements. Table 2 shows the detailed physical and material parameters used in the finite element analysis.

4.2 Finite Element Analysis Results. The normalized distributions of contact stresses along the amorphous carbon film surface at three contact states are shown in Fig. 13. At state I without

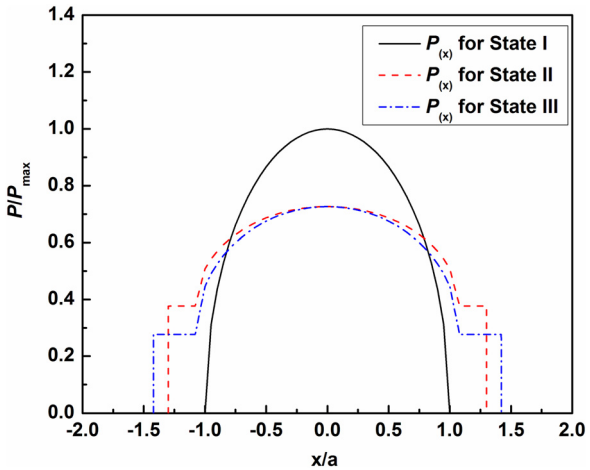

Fig. 12 Normalized pressure distributions of three contact states

the transfer layer, the analysis results agreed well with two-dimensional analytical results from other authors [31]. It is clear from Fig. 13 that the maximum contact stresses (σ_{xx}, σ_{xy}, σ_{von}) decreased as the sliding wear process went on. Figure 13(*a*) shows the distributions of surface normal stresses (σ_{xx}). The positive value of $\sigma_{xx}/P_{\max}$ gives the tensile stress of σ_{xx} and the negative value represents the compressive stress of σ_{xx}. The maximum tensile stress was about 0.35 $P_{\max}$ at state I. When the transfer layer formed, the maximum value of $\sigma_{xx}/P_{\max}$ at state II was 0.18 and that at state III was 0.10. The surface shear stress (σ_{xy}) distributions at three contact states are shown in Fig. 13(*b*), where the maximum shear stresses of all contact states were at the contact center ($x=0$), and the maximum value of $\sigma_{xy}/P_{\max}$ was 0.18 at state I, and it decreased to 0.072 and 0.036 at states II and III, respectively. The maximum values of von Mises stress also decreased with the appearance of transfer layer. The maximum values of $\sigma_{von}/P_{\max}$ were 0.30, 0.18 and 0.17 at states I, II and III respectively. In Fig. 13(*c*), it should be noted that the ratio of the peak value at the trailing edge to the maximum value at the contact center was higher at state II and then dropped down at state III, this is because when the transfer layer formed at state II, the pressure on transfer layer outside contact width changed to uniform distribution, and caused the stress concentration. Wear easily occurred at the stress concentration place, and then resulted in the decreasing of the peak value of von Mises stress at trailing edge of transfer layer at state III.

Analysis of results showed that the maximum tensile stress decreased for 71% from state I to state III, and maximum shear stress also decreased for about 80% at state III. It has been demonstrated that the mechanism for the generation of ring and tensile cracks were strongly dependent on the tensile stress at the film surface which was a mechanism of wear [32,33], while, in terms of adhesion failure during sliding contact, maintaining a low interfacial shear stress was important [34]. Von Mises stress was

Table 2 Parameters of Si_3N_4 ball, transfer layer, amorphous carbon film, and Si substrate in FEA analysis

Material	Si_3N_4 ball	Transfer layer	Amorphous carbon film	Si Substrate[c]
Elastic Modulus E/GPa	336.9	100.1	142.3	131
Density $\rho/10^3\,\mathrm{kg\cdot m^{-3}}$	3.18[a]	2.65[b]	2.65[b]	2.329
Poisson's Ratio ν	0.22[a]	0.3	0.3	0.28

[a]Reference [28].
[b]Reference [29].
[c]Reference [30].

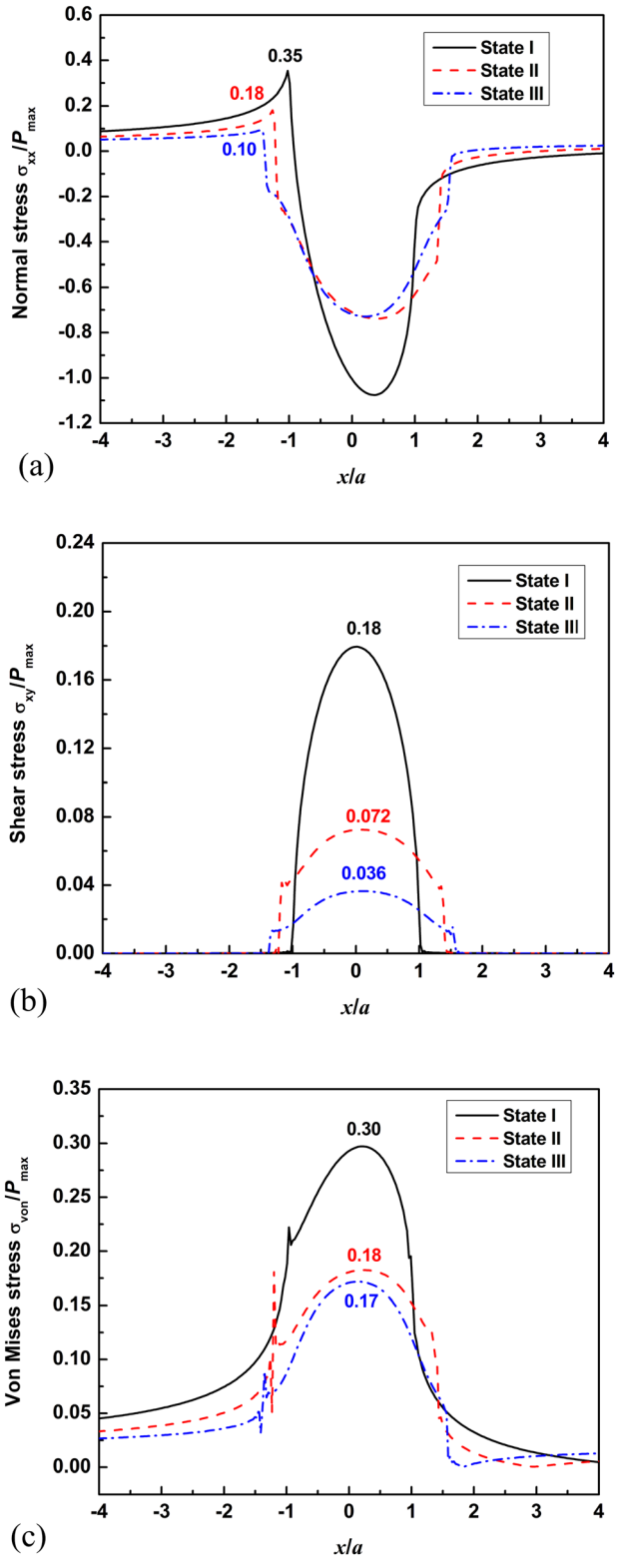

Fig. 13 Variations of normal stress σ_{xx} (*a*), shear stress σ_{xy} (*b*), and von Mises stress σ_{von} (*c*) distributions along the amorphous carbon film surface at three contact states

related to the initiation of micro-crack and the wear caused by plastic yield [35], the maximum von Mises stress also decreased from 0.30 to 0.17, with the degree of 43%. In our study, the maximum values of three contact stresses decreased with the formation and thinning of the transfer layer. Therefore, it can be concluded

that when transfer layers formed at the contact interface, they can effectively decrease the maximum contact stresses, which contributed to the long wear life of amorphous carbon film.

5 Discussion

In order to clarify the contact mechanisms of a transfer layered surface during sliding wear of amorphous carbon film, the film nano structure, mechanical property, friction coefficient, contact width, transfer layer size, and contact pressure distribution were studied and finite element analysis was used for calculating the contact stresses in the present study. Although we used the experimental observation results of the transfer layer as the source of data for the FEA model, the model may also be used as a new vision to understand transfer layer formation through discussing the effect of three contact stresses on wear mechanisms, which is related to the plastic deformation, crack initiation, and spalling of film.

In this paper, we mainly focused on the changes of contact stress distributions induced by a transfer layer, which presented a method to study the contact mechanisms of a transfer layered surface during sliding wear. The finite element model we used was two-dimensional. It is known that the contact problem for a ball sliding against a layered semi-infinite space like state I has already been studied by using two and three-dimensional numerical and finite element analysis [11,31,32], and the differences of contact stresses (normal stress, shear stress, and von Mises stress) between two and three-dimensional results were in the range from 5 to 15 percentages. When a transfer layer existed, the contact interface becomes much more complicated, and the theoretical contact model cannot be used to solve the contact mechanism. Therefore, a experimental method was used to get the characteristics of the transfer layer and a simplified analysis method was used to give the pressure distributions of different contact states. We simplified the contact models to be two-dimensional for transfer layered contact states because when a transfer layer formed at the contact interface (state II and III), the contact was similar to a block with a ball and transfer layer (as shown in Figs. 10(*b*) and 10(*c*)) sliding against the amorphous carbon film. The authors plan to conduct a more complicated study with three dimensional finite element analysis in the near future.

6 Conclusions

The contact mechanisms of a transfer layered surface during sliding wear of the Si_3N_4 ball against amorphous carbon film has been studied through experimental tests in combination with finite element analysis. As the simulation of the transfer layer at the contact interface is a complicated problem, in this paper we proposed to study the contact mechanisms with the characteristics of friction coefficients, maximum contact stresses and wear lives which were related with the transfer layers at different contact states based on the experimental results. With this method, the main conclusions are summarized by the following:

(1) The friction coefficients of amorphous carbon films during sliding wear had three stages. The initial contact stage without a transfer layer had a friction coefficient of about 0.2; the transfer layer forming stage had a friction coefficient decreasing from 0.2 to 0.05; and the transfer layered surface stable sliding stage had a friction coefficient of about 0.05.
(2) The maximum contact stresses at the surface of amorphous carbon films during sliding wear had three states, and the values decreased as the sliding wear process went on. After a transfer layer formed, the maximum tensile and shear stresses, which mainly account for the wear of film decreased for 71% and 80%, respectively, at the low friction coefficient stage (state III) compared with the initial contact state (state I). The von Mises stress also decreased for 43% during the sliding wear process.
(3) The wear life of amorphous carbon films during sliding wear was dependent on the stages of friction coefficient and the maximum contact stresses. Transfer layers formed during sliding wear and effectively decreased the friction coefficients and maximum contact stresses, ultimately contributing to the long wear life of amorphous carbon film.

Acknowledgment

The authors would like to thank the National Nature Science Foundation of China with Grant Numbers of 90923027 and 51050110137, as well as the National High-Tech Research & Develop Plan with Grant Number 2007AA04Z307 for their support.

Nomenclature

a = half contact width at state I (μm)
b = transfer layer half length (μm)
b_0 = half wear contact width (μm)
b_1 = transfer layer half length at state II (μm)
b_2 = transfer layer half length at state III (μm)
h = transfer layer thickness (μm)
h_1 = transfer layer thickness at state II (μm)
h_2 = transfer layer thickness at state III (μm)
N = friction cycle
P_0 = uniform contact pressure at states II and III (MPa)
P_b = peak contact pressure at states II and III (MPa)
P_{max} = maximum contact pressure at state I (MPa)
R = radius of the Si_3N_4 ball (mm)
V = linear speed of contact points (mm/s)
V_b = substrate bias voltage (V)
W = normal load of tribotest (N)
ρ = density ($kg \cdot m^{-3}$)
ν = Poisson's ratio
μ = friction coefficient
σ_{xx} = normal stress (MPa)
σ_{xy} = shear stress (MPa)
σ_{von} = Von Mises stress (MPa)

References

[1] Robertson, J., 2002, "Diamond Like Amorphous Carbon," Mater. Sci. and Eng., **37**, pp. 129–132.
[2] Lu, W., and Komvopoulos, K., 2001, "Nanotribological and Nanomechanical Properties of Ultrathin Amorphous Carbon Films Synthesized by Radio Frequency Sputtering," ASME J. Tribo., **123**, pp. 641–650.
[3] Erdemir, A., and Donnet, C., 2006, "Tribology of Diamond-Like Carbon Films: Recent Progress and Future Prospects," J. Phys. D: Appl. Phys., **39**, pp. R311–R327.
[4] Dickrell, P. L., Argibay, N., Erylimaz, O. L., Erdemir, A., and Sawyer, W. G., 2009, "Temperature and Water Vapor Pressure Effects on the Friction Coefficient of Hydrogenated Diamond Like Carbon Films," ASME J. Tribo., **131**, p. 032102.
[5] Eryilmaz, O. L., and Erdemir, A., 2008, "TOF-SIMS and XPS Characterization of Diamond-Like Carbon Films After Tests in Inert and Oxidizing Environments," Wear, **265**, pp. 244–254.
[6] Heimberg, J. A., Wahl, K. J., Singer, I. L., and Erdemir, A., 2001, "Superlow Friction Behavior of Diamond-Like Carbon Coatings: Time and Speed Effects," Appl. Phys. Lett., **78**, pp. 2449–2451.
[7] Sugimoto, I., and Miyake, S., 1990, "Oriented Hydrocarbons Transferred From a High Performance Lubricative Amorphous C:H:Si Film During Sliding in a Vacuum," Appl. Phys. Lett., **56**, pp. 1868–1870.
[8] Fukui, H., Irie, M., Utsumi, Y., Oda, K., and Ohara, H., 2001, "An Investigation of the Wear Track on DLC (a-C:H) Film by Time-Of-Flight Secondary Ion Mass Spectroscopy," Surf. Coat. Technol. **146**, pp. 378–383.
[9] Holmberg, K., Ronkainen, H., and Laukkanen, A., 2007, "Friction and Wear of Coated Surfaces—Scales, Modelling and Simulation of Tribomechanisms," Surf. Coat. Technol., **202**, pp. 1034–1049.
[10] Scharf, T. W., and Singer, I. L., 2009, "Role of Transfer Film on the Friction and Wear of Metal Carbide Reinforced Amorphous Carbon Coatings During Run-in," Tribo. Lett., **36**, pp. 43–53.
[11] O'Sullivan, T. C., and King, R. B., 1988, "Sliding Contact Stress Field Due to a Spherical Indenter on a Layered Elastic Half-Space," ASME J. Tribo., **110**, pp. 235–240.
[12] Diao, D. F., Sawaki, Y., and Suzuki, H., 1996, "Effect of Interlayer on Maximum Contact Stresses of Hard Coating Under Sliding Contact," Surf. Coat. Technol., **86–87**, pp. 480–485.
[13] Diao, D. F., Kato, K., and Hayashi, K., 1994, "The Maximum Tensile Stress on a Hard Coating Under Sliding Friction," Tribol. Inter., **27**, pp. 267–272.

[14] Ye, N., and Komvopoulos, K., 2003, "Three-Dimensional Finite Element Analysis of Elastic-Plastic Layered Media Under Thermomechanical Surface Loading," ASME J. Tribo., **125**, pp. 52–59.
[15] Cai, S. B., and Bhushan, B., 2007, "Three-Dimensional Sliding Contact Analysis of Multilayered Solids With Rough Surfaces," ASME J. Tribo., **129**, pp. 40–59.
[16] Wang, Z. J., Wang, W. Z., Wang, H., Zhu, D., and Hu, Y. Z., 2010, "Partial Slip Contact Analysis on Three-Dimensional Elastic Layered Half Space," ASME J. Tribo., **132**, p. 021403.
[17] Kadiric, A., Sayles, R. S., Zhou, X. B., and Ioannides, E., 2003, "A Numerical Study of the Contact Mechanics and Sub-Surface Stress Effects Experienced Over a Range of Machined Surface Coatings in Rough Surface Contacts," ASME J. Tribo., **125**, pp. 720–730.
[18] Ye, N., and Komvopoulos, K., 2003, "Effect of Residual Stress in Surface Layer on Contact Deformation of Elastic-Plastic Layered Media," ASME J. Tribo., **125**, pp. 692–699.
[19] Kadiric, A., Sayles, R. S., and Ioannides, E., 2008, "Thermo-Mechanical Model for Moving Layered Rough Surface Contacts," ASME J. Tribo., **130**, p. 011016.
[20] Jiang, W. F., and Diao, D. F., 2010, "The Critical Conditions for Tribo-Demagnetization of Perpendicular Magnetic Recording Disk Under Sliding Contact," ASME J. Tribo., **132**, p. 021901.
[21] Chhowalla, M., Ferrari, A. C., Robertson, J., and Amaratunga, G. A. J., 2000, "Evolution of sp^2 Bonding With Deposition Temperature in Tetrahedral Amorphous Carbon Studied by Raman Spectroscopy," Appl. Rhys. Lett., **76**, pp. 1419–1421.
[22] Miyoshia, K., Richard, L.C. W., and Garscaddenc, A., 1992, "Friction and Wear of Diamond and Diamondlike Carbon Coatings," Surf. Coat. Technol., **54–55**, pp. 428–434.
[23] Tokoroyama, T., Goto, M., Umehara, N., Nakamura, T., and Honda, F., 2003, "Effect of Nitrogen Atoms Desorption on the Friction of the CN_x Coating Against Si_3N_4 Ball in Nitrogen Gas," Tribo. Lett., **22**, pp. 215–220.
[24] Tokoroyama, T., Umehara, N., Tomita, H., and Takenoshita Y., 2003, "Effect of Surface Roughness and Transfer Layer of Mating Ceramic Parts for Ultra Low Friction Phenomena in Sliding Between CN_x and Ceramics," Trans. Jpn. Soc. Mech. Eng., **69**, pp. 2824–2829.
[25] Oliver, W. C., and Pharr, G. M., 1992, "An Improved Technique for Determining Hardness and Elastic Modulus Using Load and Displacement Sensing Indentation Experiments," J. Mater. Res., **7**, pp. 1564–1583.
[26] Ding, J., Leen, S. B., and McColl, I. R., 2004, "The Effect of Slip Regime on Fretting Wear-Induced Stress Evolution," Inter. J. Fatigue, **26**, pp. 521–531.
[27] Nowell, D., 2010, "Simulation of Fretting Wear in Half-Plane Geometries-Part II: Analysis of the Transient Wear Problem Using Quadratic Programming," ASME J. Tribo., **132**, p. 021402.
[28] Bhushan, B., 1996, *Tribology and Mechanics of Magnetic Storage Devices*, Springer-Verlag Press, New York, USA.
[29] Ferrari, A. C., Libassi, A., and Tanner, B. K., 2000, "Density, sp^3 Fraction, and Cross-Sectional Structure of Amorphous Carbon Films Determined by X-Ray Reflectivity and Electron Energy-Loss Spectroscopy," Phys. Rev. B, **62**, pp. 11089–11103.
[30] Bhushan, B., Liu, H. W., and Stephen, M. Hsu., 2004, "Adhesion and Friction Studies of Silicon and Hydrophobic and Low Friction Films and Investigation of Scale Effects," ASME J. Tribo., **126**, pp. 583–590.
[31] King, R. B., and O'Sullivan, T. C., 1987, "Sliding Contact Stresses in a Two-Dimensional Layered Elastic Half Space," Int. J. Solids Struct., **23**, pp. 581–597.
[32] Diao, D. F., Kato, K., and Hokkirigawa, K., 1994, "Fracture Mechanisms of Ceramic Coatings in Indentation," AMSE J. Tribo., **116**, pp. 860–869.
[33] Johnson, K. L., 1984, *Contact Mechanics*, Cambridge University Press, Cambridge, UK, Chap. 4.
[34] Diao, D. F., and Sawaki, Y., 1995, "Fracture Mechanisms of Ceramic Coating During Wear," Thin Solid Films, **270**, pp. 362–366.
[35] Tangena, A. G., Wijnhoven, P. J. M., and Muijderman, E. A., 1988, "The Role of Plastic Deformation in Wear of Thin Film," ASME J. Tribo., **110**, pp. 602–608.